Threshold photodetachment spectroscopy of the astrochemical anion CN⁻

Cite as: J. Chem. Phys. **153**, 184309 (2020); https://doi.org/10.1063/5.0029841 Submitted: 16 September 2020 . Accepted: 28 October 2020 . Published Online: 12 November 2020

D Malcolm Simpson, Markus Nötzold, Alice Schmidt-May, D Tim Michaelsen, Björn Bastian, D Jennifer Meyer, Robert Wild, Franco A. Gianturco, Milan Milovanović, D Viatcheslav Kokoouline, and D Roland Wester









ARTICLES YOU MAY BE INTERESTED IN

The nature of the chemical bond in the dicarbon molecule

The Journal of Chemical Physics 153, 164301 (2020); https://doi.org/10.1063/5.0023067

Excited-state dynamics of CH₂I₂ and CH₂IBr studied with UV-pump VUV-probe momentum-resolved photoion spectroscopy

The Journal of Chemical Physics 153, 184304 (2020); https://doi.org/10.1063/5.0026177

Photodissociation spectroscopy of N_2O^{\dagger} in the ion storage ring RICE

The Journal of Chemical Physics 153, 184305 (2020); https://doi.org/10.1063/5.0027805



Learn how to perform the readout of up to 64 qubits in parallel

With the next generation of quantum analyzers on November 17th





Threshold photodetachment spectroscopy of the astrochemical anion CN⁻

Cite as: J. Chem. Phys. 153, 184309 (2020); doi: 10.1063/5.0029841 Submitted: 16 September 2020 • Accepted: 28 October 2020 •







Published Online: 12 November 2020

Malcolm Simpson,¹ Markus Nötzold,¹ Alice Schmidt-May,^{1,a)} Tim Michaelsen,¹ Björn Bastian,^{1,b)}
Jennifer Meyer,¹ Robert Wild,¹ Franco A. Gianturco,¹ Milan Milovanović,² Viatcheslav Kokoouline,³

and Roland Wester^{1,c)}

AFFILIATIONS

- ¹Institut für Ionenphysik und Angewandte Physik, Universität Innsbruck, Technikerstraße 25, 6020 Innsbruck, Austria
- ²University of Belgrade, Faculty of Physical Chemistry, Studentski trg 12-16, P.O. Box 47, 11158 Belgrade, Serbia
- ³Department of Physics, University of Central Florida, 4111 Libra Drive, Physical Sciences Bldg. 430, Orlando, Florida 32816-2385, USA
- Present address: Department of Physics, Stockholm University, AlbaNova, SE-106 91 Stockholm, Sweden.
- ^{b)}Present address: Department of Physics and Astronomy, Aarhus University, Ny Munkegarde 120, 8000 Aarhus C, Denmark.
- a) Author to whom correspondence should be addressed: roland.wester@uibk.ac.at

ABSTRACT

Threshold photodetachment spectroscopy has been performed on the molecular anion CN^- at both 16(1) K and 295(2) K in a 22-pole ion trap and at 295(2) K from a pulsed ion beam. The spectra show a typical energy dependence of the detachment cross section yielding a determination of the electron affinity of CN to greater precision than has previously been known at 31 163(16) cm⁻¹ [3.864(2) eV]. Allowed s-wave detachment is observed for CN^- , but the dependence of the photodetachment cross section near the threshold is perturbed by the long-range interaction between the permanent dipole moment of CN and the outgoing electron. Furthermore, we observe a temperature dependence of the cross section near the threshold, which we attribute to a reduction of the effective permanent dipole due to higher rotational excitation at higher temperatures.

© 2020 Author(s). All article content, except where otherwise noted, is licensed under a Creative Commons Attribution (CC BY) license (http://creativecommons.org/licenses/by/4.0/). https://doi.org/10.1063/5.0029841

I. INTRODUCTION

Molecule-photon and molecule-electron collisions are a fundamental process in many physical and chemical systems and are prevalent in areas such as atmospheric chemistry and astrochemistry and technical environments such as semiconductor manufacture, combustion chemistry, and fusion plasmas. Photodetachment of the extra electron in negatively charged ions provides a sensitive probe of the interaction between a single electron and the neutral molecule, uncovering electron correlation effects that are shielded by the long-range Coulomb potential in the case of photoionization. Historically, photodetachment has been used to determine accurate electron affinities of neutral species and for investigation of excited anionic states. More recently, threshold photodetachment has been used to study chemical reaction dynamics in terms of electron

rearrangement and to probe the transition state.⁴ The technique has also been used as a probe for terahertz spectroscopy,^{5,6} as a measure of cold collisional kinetics,⁷ to perform rotational thermometry,⁸ and to observe electronic transitions in the detachment spectrum of astrochemically relevant species.^{9,10}

The cross section for threshold photodetachment is in general well described by a Wigner-type law, ¹¹ the shape of which is determined by the angular momentum taken away by the outgoing electron. A number of theoretical studies have so far focused on deviations from this law for the case of dipolar neutral parent molecules. An analytical model describing the divergence from the Wigner law in terms of dipole strength ^{12,13} has been developed. For the case in which the dipole strength sufficiently dominates the electronic angular momentum, it has been shown ¹⁴ that the detachment cross section yields an oscillatory behavior at the threshold. For the

case of dipoles that exceed a critical value of \sim 1.67 D, dipole bound states can exist close to the detachment threshold. 15,16

The cyanide anion (CN⁻) is an interesting subject for study due to its $^{1}\Sigma^{+}$ closed shell structure and a large electron affinity of the parent radical. Photoelectron spectroscopy of CN was presented by Bradforth et al., 17 and the electron affinity of CN was determined to be 3.862(4) eV. The CN molecule has a permanent dipole of ~1.45 D, 18 which is subcritical for the formation of dipole bound states and the occurrence of an oscillatory cross section at the threshold but suitably large to result in a modification of the Wigner threshold law. CN was used in astrochemical models of both the dark molecular cloud TMC-1 and the circumstellar envelope of the carbon-rich star IRC + 10216¹⁹ and was observed in the latter²⁰ in 2010. CN is also the dominant negative ion observed in Titan's atmosphere. 21,22 Absolute photodetachment cross section measurements of CN⁻ were performed by our group in 2013,²³ and it was shown that photodetachment is the primary destruction mechanism for this species in circumstellar environments.

Cold molecular ions have been studied primarily in either cryogenic storage rings^{24,25} or multipole ion traps, ^{7,26} both of which allow for mass selectivity combined with long storage and hence exposure times. In this work, we perform threshold photodetachment spectroscopy of CN⁻ at 16 K buffer gas temperature and at room temperature in our 22-pole cryogenic ion trap and at room temperature from the ion beam in our crossed-beam velocity map imaging (VMI) setup. In Sec. II, we derive a model for threshold photodetachment from first principles, and in Sec. III, the two experimental setups used in this study are described. In Sec. IV, we discuss the results of measurements on CN⁻ and use the model derived in Sec. II to improve upon the determination of the electron affinity of CN and to investigate the effect of the CN dipole moment on the Wigner threshold law.

II. THEORY

The photodetachment cross section from an initial state $|i\rangle$ to a final state $|f\rangle$ is given by 27

$$\sigma_{PD} = \frac{4\pi^2 \omega}{c} \cdot \left| \left\langle f | \overrightarrow{\epsilon} \cdot \overrightarrow{d} | i \right\rangle \right|^2, \tag{1}$$

where ω is the photon frequency, $\overrightarrow{\epsilon}$ is the polarization vector, and \overrightarrow{d} is the dipole operator. The factor $4\pi^2\omega/c$ corresponds to energy normalization. For a linear rigid rotor within the Born-Oppenheimer approximation, the states may be written in the form

$$|i\rangle = \sqrt{\frac{2J'' + 1}{8\pi^2}} D_{m'',0}^{J''*}(\alpha\beta\gamma)\chi''\phi'',$$
 (2)

$$|f\rangle = \sqrt{\frac{2J'+1}{8\pi^2}} D_{m',0}^{J'*}(\alpha\beta\gamma)\chi'\phi',$$
 (3)

in which $D_{m,0}^{J*}(\alpha\beta\gamma)$ is a Wigner D matrix and J and m are the total angular momentum and its projection, respectively. χ is the eigenfunction of the molecular vibration, and ϕ is that of the electronic coordinates

It is easier to evaluate the cross section of Eq. (1) in the molecular frame. Assuming that laser polarization is along the z-axis in the

lab frame, the dipole transition operator is written as

$$\overrightarrow{\epsilon} \cdot \overrightarrow{d} = d_z = \sum_{k=-1}^{1} d_k D_{0,k}^{1*}, \tag{4}$$

and the matrix element of the transition moment becomes

$$\langle f|\overrightarrow{\epsilon}\cdot\overrightarrow{d}|i\rangle = \sum_{k=-1}^{1} \langle D_{m',0}^{J'*}|D_{0,k}^{1*}|D_{m'',0}^{J''*}\rangle$$

$$\cdot \sqrt{\frac{(2J''+1)(2J'+1)}{(8\pi^{2})^{2}}} \cdot \langle \chi'|\chi''\rangle \cdot \langle \phi'|d_{k}|\phi''\rangle. \quad (5)$$

The product of three Wigner D functions may be represented by a product of two Clebsch–Gordan coefficients by making use of the relation²⁸

$$\langle D_{m',0}^{J'*}|D_{0,k}^{1*}|D_{m'',0}^{J'''*}\rangle = \frac{8\pi^2}{2J'+1} \cdot C_{J'',m'',1,0}^{J',m'} \cdot C_{J'',0,1,k}^{J',0}. \tag{6}$$

Noting that the final Clebsch–Gordan coefficient is only non-zero for the case k = 0, the photodetachment cross section between states with different values of m is thus written as

$$\sigma_{PD}^{m',m''} = \frac{4\pi^2 \omega}{c} \cdot \frac{2J'' + 1}{2J' + 1} \cdot |C_{J'',m'',1,0}^{J',m'}|^2 \cdot |C_{J'',0,1,0}^{J',0}|^2$$
$$\cdot |\langle \chi' | \chi'' \rangle|^2 \cdot |\langle \phi' | d_0 | \phi'' \rangle|^2. \tag{7}$$

By summing over all possible orientations m and dividing through by 2J''+1 to account for the degeneracy, we are led to the cross section

$$\sigma_{PD} = \frac{1}{2J'' + 1} \sum_{w'} \sum_{w''} \sigma_{PD}^{m',m''}.$$
 (8)

Noting that the only term that depends on the orientation m is the first Clebsch–Gordan coefficient, the double sum may be reduced to a single term by the evaluation

$$\sum_{m'} \sum_{m''} |C_{J'',m'',1,0}^{J',m'}|^2 = \frac{2J'+1}{3}.$$
 (9)

The further simplified cross section now has the form

$$\sigma_{PD} = \frac{4\pi^2 \omega}{3c} \cdot |C_{J'',0,1,0}^{J',0}|^2 \cdot |\langle \chi' | \chi'' \rangle|^2 \cdot |\langle \phi' | d_0 | \phi'' \rangle|^2. \tag{10}$$

Next, one has to take into account the rotational population of the thermalized ion ensemble at temperature T by inserting the weights

$$W_{J,T} = \frac{(2J''+1) \cdot e^{-\frac{E_{rot}}{kT}}}{\sum_{J} (2J''+1) \cdot e^{-\frac{E_{rot}}{kT}}}.$$
 (11)

We then replace the constant vibrational Franck–Condon factor and the electronic part of the transition matrix element at the threshold with the Wigner law given by $(E_{ph} - E_{th})^P$, where E_{th} is the energy at each rotational threshold,

$$E_{th} = E_{EA} - B'' \cdot J''(J'' + 1) + B' \cdot J'(J' + 1), \tag{12}$$

and P is a system-dependent component we shall further discuss below. The rotational constants for CN and CN⁻, B' = 1.90 and B'' = 1.87, were taken from Refs. 29 and 30, respectively.

By dropping the constant prefactors, the final relative cross section suitable for simulation has the form

$$\sigma_{\text{PD}}(E) \propto \sum_{j''=0}^{J_{\text{max}}} \sum_{j''=0}^{J_{\text{max}}} W_{j'',T} \cdot |C_{j''010}^{j'0}|^2 \cdot (E_{\text{ph}} - E_{\text{th}})^P \cdot \Theta(E_{\text{ph}} - E_{\text{th}}), \tag{13}$$

where $\Theta(E_{\rm ph}-E_{\rm th})$ is the Heaviside function ensuring only transitions with $E_{ph}>E_{\rm th}$ are considered.

For an atom or non-polar molecule, the exponent P on the Wigner threshold law is equal to l+1/2, where l is the angular momentum taken away by the outgoing electron. However, for neutral molecules with a permanent dipole moment, the electron–dipole interaction mixes different partial waves, and we write the exponent in the form $P = \lambda + 1/2$, where λ is generally non-integer.

III. EXPERIMENT

Threshold photodetachment spectroscopy of CN⁻ has been performed in two different setups. Room temperature [295(2) K] measurements were taken in our velocity map imaging (VMI) setup in which VMI was used to detect the intensity of the electron signal after photodetachment from the ion beam. More detailed measurements were performed in our 22-pole ion trap setup repeating those at room temperature and also at cryogenic temperature [16(1) K]. In both cases, CN⁻ and other masses are produced in a pulsed plasma discharge within a supersonic expansion of acetonitrile (CH₃CN) in an argon carrier gas. CN⁻ is then projected along the axis of the experiment by pulsing a set of Wiley–McLaren style electrodes.

A. 22-Pole ion trap setup

The 22-pole radiofrequency ion trap setup has been reported previously. CN ions are selectively loaded from the time-of-flight separated masses into the trap by pulsing the hollow cylindrical end-cap electrode and blocking the access of both heavier and lighter species. Improved stability of the ion signal is undertaken by performing the loading operation a number of times for each experimental cycle.

The ion trap is mechanically fixed to a closed cycle helium cryostat allowing the trap temperatures to be tuned between room temperature and about 10 K. A few hundred to a few thousand ions are loaded into the trap and thermalized with the trap temperature through application of a helium buffer gas with particle densities on the order of 10¹¹/cm³. Numerical simulations have shown that thermalization is complete after a few tens of milliseconds of trapping, and a pre-trapping period of 300 ms has been allowed for in this work. In recent studies with the OH⁻ ion, it has been shown that complete thermalization of the internal energies of the ions is not achieved. Instead, rotational temperatures were found to be larger by about 10 K at the coldest trap temperatures.³² A similar increase, which we attribute at least in parts to the existence of patch potentials on the rf electrodes, is probably also occurring in the present experiment.

After thermalization, the ions are exposed to the photodetachment laser for 10 s. The laser is then switched off before the ions are extracted from the trap in order to eliminate spurious results due to the Doppler effect upon extraction. Following exposure and trapping, the ions are released from the trap through the same end-cap electrode and are guided toward a microchannel plate (MCP) detector, where they are identified by time-of-flight. The photon energy dependent depletion of the trapped ion signal is then measured. We alternate photodetachment with background measurements in which the ions are trapped for 0.1 s without irradiation providing a measure of the long term stability of the ion signal. The UV beam intensity is measured by a bolometer to account for intensity fluctuations.

B. Crossed-beam imaging setup

The VMI setup has been extensively described elsewhere,³³ and only the necessary details will be reported here. The setup is primarily used for the study of reaction dynamics in crossed-beam ionmolecule collisions by measuring energy distributions in the product ions.34,35 In the present experiment, a CN beam is released from the pulsed ion source at a repetition rate of 20 Hz. The time-of-flight separated ion packets are guided into an octupole radiofrequency ion trap for thermalization at room temperature through collisions with a N₂ buffer gas. Loading of the trap is gated such that only CN is confined and all other masses are blocked from access to the downstream parts of the experiment. After thermalization, the ions are released from the trap and guided into the interaction region in which they are crossed with a high intensity pulsed UV laser beam with a repetition rate of 10 Hz, allowing for both a foreground and a background signal consisting of the ion beam only. Together with the laser interaction, the VMI potentials are switched on to accelerate all negatively charged species upward toward an MCP detector with a phosphor screen resulting in a spatial distribution of localized light pulses, which is recorded by a CCD camera. By gating the MCP detector for the arrival of electrons, the impact signals from all other, much more massive, particles can be eliminated. The background ion signal is measured on an MCP detector colinear with the ion beam immediately following the interaction region. It provides a measure of the long term stability of the ion signal. The trajectory of the remaining CN following photodetachment is deflected due to the switching on of VMI, and so a direct measurement of the ion signal from the photodetached beam was not possible. The laser pulse energy is monitored by dumping the pulse into a bolometer after interaction. This is sufficient for monitoring the relative strength of the photodetachment signal as the number of ion-photon interactions is negligible in comparison with the total number of photons in a single pulse.

C. Photodetachment laser system

The laser setup was identical in both cases and consists of a frequency-doubled pulsed dye laser (Radiant Dyes Narrow Scan), which is pumped by the second harmonic of a 50 Hz pulsed Nd:YAG laser (Spectra Physics). The dye used is DCM dissolved in ethanol, and the frequency doubled output produces a scanning range of 306 nm–336 nm in order to cover the threshold region of CN⁻ with an expected threshold at 321 nm. The UV beam is guided to

the setup through free space and passed into the vacuum chamber through a fused silica window.

In the case of the VMI setup, the laser is aligned perpendicular to the pulsed CN⁻ beam, while in the trap setup, the laser propagates along the axis of the trap, entering and exiting through the end-cap electrodes. To synchronize with the VMI experiment, the laser repetition rate has been reduced to 10 Hz.

IV. RESULTS AND DISCUSSION

A. Photodetachment spectra

Threshold photodetachment of $\operatorname{CN}^-(X^1\Sigma^+) + hv \to \operatorname{CN}(X^2\Sigma^+) + e^-$ has been measured at both 16(1) K and 295(2) K in our 22-pole ion trap and at 295(2) K from the pulsed ion beam in our VMI setup. The relative cross sections plotted against the photon energy for the 16 K and 295 K measurements are shown in Figs. 1 and 2, respectively. For the 22-pole trap setup, Figs. 1 and 2 show the photodetachment signal obtained by subtracting the photon dependent depletion signal from a first order polynomial fit to the alternatingly measured ion background. The resultant photodetachment signal is then normalized to the laser pulse energy. For the case of photodetachment from the ion beam, the signal is determined from the integral counts of the electron impacts on the VMI detector and presented as a function of the photon energy. This signal is normalized both to the ion intensity and to the laser pulse energy.

In each case, the cross sections are fitted to the model derived in Sec. II [Eq. (13)]. For the case of the 16 K ion trap measurement, the CN electron affinity, the exponent on the Wigner threshold law, and the proportionality constant have been left as free parameters. The electron affinity determination from the room temperature measurements however is less robust due to rotational excitation leading to a more shallow onset of the threshold region. In this case, the electron affinity has been fixed to the value determined from the

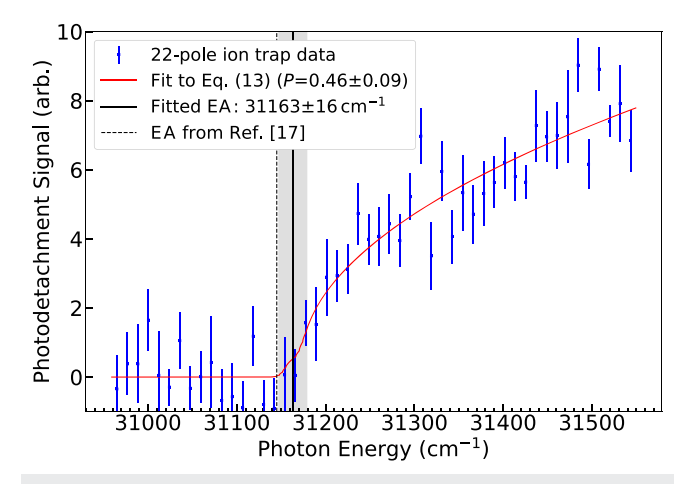


FIG. 1. Relative photodetachment cross section of CN $^-$ at 16 K buffer gas measured in the 22-pole ion trap setup; the plotted uncertainties are 1σ error bars. The data points are fitted to the model of Eq. (13) with the electron affinity (EA) of CN, the exponent P, and the overall scaling factor in the Wigner threshold law provided as free parameters.

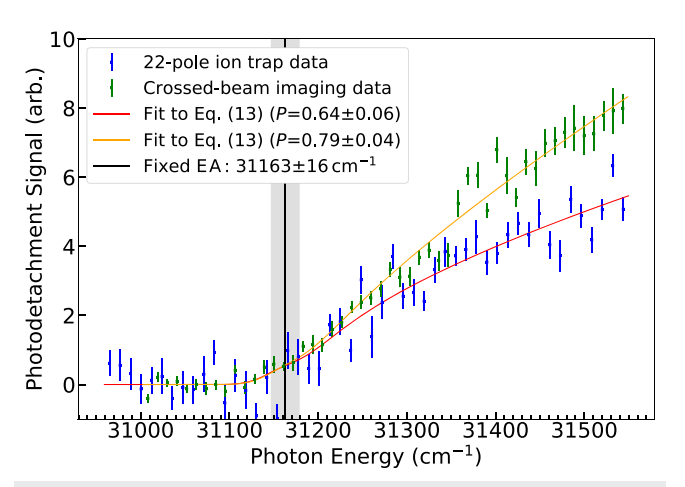


FIG. 2. Relative photodetachment cross section of CN $^-$ at 295 K buffer gas measured in the 22-pole ion trap setup and in the crossed-beam imaging setup; the plotted uncertainties are 1σ error bars. The Wigner law exponent and scaling factors are left as free fit parameters, while the electron affinity (EA) of CN is fixed to the value determined by the 16 K measurement.

cryogenic ion trap. The fitted parameters are listed in Figs. 1 and 2 and discussed below.

B. The electron affinity of the CN molecule

The electron affinity of CN is obtained from the cross section fit to the 16 K data (see Fig. 1). In fitting the data, it is necessary to consider the range of validity of the Wigner threshold law. Due to the presence of the sharp threshold behavior in this measurement, the determination of the electron affinity has been found to be robust to applying the fitting routine over different ranges. We obtain a value for the CN electron affinity from this dataset of 31 163(16) cm⁻¹ [3.864(2) eV].

The quoted accuracy is determined by a combination of the statistical accuracy of the fit $(14~{\rm cm}^{-1})$ and systematic effects due to the expected incomplete thermalization of the rotational temperature of the ions with that of the trap. This has been dealt with by performing the fit over a range of rotational temperatures contributing a further $2~{\rm cm}^{-1}$ to the overall error budget. Further systematic effects due to the pointing stability of the laser propagating through free space were noted to affect the high energy region above $31~550~{\rm cm}^{-1}$, which have therefore not been included in the fit.

The determined electron affinity is in excellent agreement with the best previously determined value of 3.862(4) eV¹⁷ and improves the achieved accuracy by a factor of two.

C. The exponent in the Wigner threshold law

For atoms and non-polar molecules, the exponent P=l+1/2 in the Wigner threshold law describes the angular momentum l taken away by the outgoing electron. The detachment channel with l=0, referred to as the s-wave, is barrierless and dominates the detachment profile in cases where symmetry considerations allow this. Higher order partial waves, however, experience an increasing centrifugal barrier hindering these detachment channels. In the case

of polar molecules, different partial waves become mixed yielding $P = \lambda + 1/2$, where λ is no longer an integer value.

s-wave detachment is allowed for CN $^-$, and the value of P=0.46(9) that has been determined from the 16 K ion trap measurement (see Fig. 1) agrees with the theoretical expectation of $P\approx0.44$, 36 in which the outgoing electron interacts with a neutral molecule with the angular momentum and its projection of $J=\frac{1}{2}$ and $\Omega=\frac{1}{2}$, respectively. The accuracy of the experimentally determined P-value is finite, but fitting the cross section over different ranges of the dataset consistently yields values of P<0.5. This changes for the data measured at room temperature, where a value of P=0.64(6) is measured. This deviation, which is difficult to understand with the cross section model introduced above, is supported by the measurement carried out with the VMI setup, which yields a value of P=0.79(4).

The emergence of higher order partial waves as an explanation for the large *P*-value can be excluded, as the centrifugal barrier experienced by a *p*-wave electron is too large to overcome. The effective potential for a polar molecule has the form

$$V_{\text{eff}} = -\frac{\alpha e^2}{2(4\pi\epsilon_0)^2 r^4} + \frac{\hbar^2 l(l+1)}{2\mu r^2} - \frac{de\cos(\theta)}{4\pi\epsilon_0 r^2},$$
 (14)

where α is the molecular polarizability, $\mu \approx m_e$ is the reduced mass, d is the dipole moment, and θ is the orientation of the molecule with respect to the outgoing electron. Calculating $V_{\rm eff}$ for the CN- e^- system and for the geometrical extremes of $\cos(\theta)=\pm 1$ gives the range of barrier heights a p-wave electron must cross. Results of the calculations are shown in Fig. 3 in which the electron—molecule separation distance is plotted against $V_{\rm eff}$ for both an s-wave and a p-wave electron. As can be seen from Fig. 3, even the minimum barrier height is energetically beyond the maximum photoelectron energy produced in the photodetachment measurements. That is, although p-wave and higher orders are included in the partial wave expansion, only the s-wave detachment is observable in our experiment.

For pure *s*-wave detachment, a *P*-value above 0.5 is difficult to rationalize. Enhanced rotation is expected to result in a reduction of the effective dipole so that the Wigner law returns to the atomic case of $P = \lambda + 1/2 = l + 1/2 = 0.5$. For the case of electrons interacting with

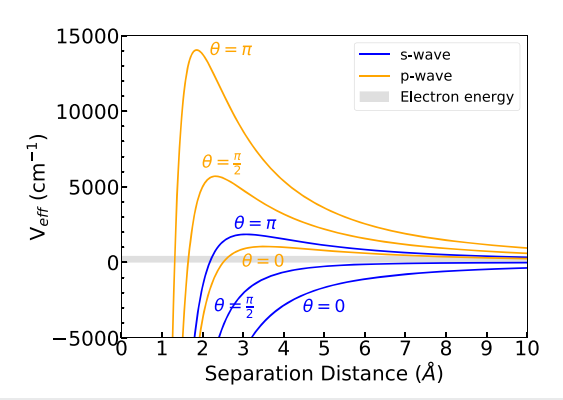


FIG. 3. Effective potential of the CN–e⁻ system for both an s-wave and a *p*-wave electron. The maximum centrifugal barrier heights for the *p*-wave detachment channel for different molecule–electron geometries are highlighted.

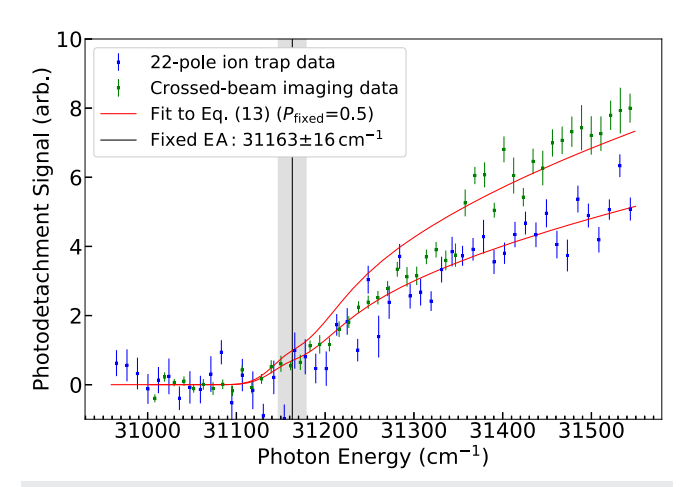


FIG. 4. Relative photodetachment cross section at 295 K of CN $^-$ measured in the 22-pole ion trap setup and in the crossed-beam imaging setup (the same data as in Figs. 1 and 2). Here, both the electron affinity (EA) of CN and the Wigner exponent are fixed to the value determined by the 16 K measurement and the theoretical expectation of 0.5, respectively, and only the vertical scaling factor has been fitted.

a rotating CN molecule, we have estimated that the increased rotational excitation of CN^- at room temperature is sufficient for the average dipole term to approach zero. The effective potential therefore begins to approximate a non-dipolar system, i.e., a spherical interaction potential.

This shows that the maximum value of the Wigner exponent under these conditions is predicted to be limited to P=0.5. We have therefore performed comparisons of our 295 K data with the cross section model where the electron affinity is fixed as before but also P is fixed to the expected value of 0.5. The results are shown in Fig. 4. Clearly, the data do not give the appearance of being fit in Fig. 2; however, it cannot be denied that also choosing P=0.5 is compatible with the datasets. An accurate quantum dynamics treatment of the outgoing electron in the dipolar potential would be desirable to shed further light on this behavior.

V. CONCLUSION

In this work, we have presented a model and experimental results on threshold photodetachment spectroscopy of the molecular anion CN⁻ at both room temperature in our crossed-beam imaging and 22-pole ion trap setups and 16 K in our ion trap setup. We have been able to describe the low-temperature photodetachment cross section near the threshold with the quantum mechanical model that takes into account the charge–dipole interaction of the outgoing electron. In doing so, we have narrowed down the determination of the electron affinity of CN to 31 163(16) cm⁻¹. In comparison with *ab initio* computations, such an improved value of a molecular electron affinity will aid in a better understanding of electronic correlation effects in gas-phase ion chemistry.

In addition, the temperature-dependent detachment spectra have allowed us to uncover a dependence of the Wigner threshold law on the rotational excitation of the molecule, which is only in part explained with the present model for the cross section near the threshold. Quantum dynamical modeling of a permanent dipole with different rotational distributions is required in order to better understand this behavior and to clarify if *p*-wave detachment may contribute to the measured signal.

ACKNOWLEDGMENTS

This work was supported by the Austrian Science Fund (FWF) through the Doctoral Programme Atoms, Light, and Molecules, Project No. W1259-N27, and through Project No. P27047-N20.

DATA AVAILABILITY

The data that support the findings of this study are available from the corresponding author upon reasonable request.

REFERENCES

- ¹D. J. Pegg, Nucl. Instrum. Methods Phys. Res., Sect. B **99**, 140 (1995).
- ²D. M. Wetzel and J. I. Brauman, Chem. Rev. **87**, 607 (1987).
- ³ R. E. Continetti and H. Guo, Chem. Soc. Rev. 46, 7650 (2017).
- ⁴D. M. Neumark, Phys. Chem. Chem. Phys. 7, 433 (2005).
- ⁵S. Lee, D. Hauser, O. Lakhmanskaya, S. Spieler, E. S. Endres, K. Geistlinger, S. S. Kumar, and R. Wester, Phys. Rev. A **93**, 032513 (2016).
- ⁶O. Lakhmanskaya, M. Simpson, S. Murauer, M. Nötzold, E. Endres, V. Kokoouline, and R. Wester, Phys. Rev. Lett. 120, 253003 (2018).
- ⁷D. Hauser, S. Lee, F. Carelli, S. Spieler, O. Lakhmanskaya, E. S. Endres, S. S. Kumar, F. Gianturco, and R. Wester, Nat. Phys. 11, 467 (2015).
- ⁸R. Otto, A. von Zastrow, T. Best, and R. Wester, Phys. Chem. Chem. Phys. 15, 612 (2013).
- ⁹T. Pino, M. Tulej, F. Güthe, M. Pachkov, and J. P. Maier, J. Chem. Phys. 116, 6126 (2002).
- ¹⁰T. Best, R. Otto, S. Trippel, P. Hlavenka, A. von Zastrow, S. Eisenbach, S. Jézouin, R. Wester, E. Vigren, M. Hamberg, and W. D. Geppert, Astrophys. J. 742, 63 (2011).
- ¹¹E. P. Wigner, Phys. Rev. **73**, 1002 (1948).
- ¹²P. C. Engelking, Phys. Rev. A 26, 740 (1982).
- ¹³D. R. Herrick and P. C. Engelking, Phys. Rev. A 29, 2421 (1984).
- ¹⁴T. F. O'Malley, Phys. Rev. 137, A1668 (1965).
- ¹⁵W. R. Garrett, J. Chem. Phys. 77, 3666 (1982).

- ¹⁶F. Carelli, F. A. Gianturco, R. Wester, and M. Satta, J. Chem. Phys. **141**, 054302 (2014).
- ¹⁷S. E. Bradforth, E. H. Kim, D. W. Arnold, and D. M. Neumark, J. Chem. Phys. 98, 800 (1993).
- ¹⁸R. Thomson and F. W. Dalby, Can. J. Phys. **46**, 2815 (1968).
- ¹⁹T. J. Millar, C. Walsh, and T. A. Field, Chem. Rev. 117, 1765 (2017).
- ²⁰ M. Agúndez, J. Cernicharo, M. Guélin, C. Kahane, E. Roueff, J. Kłos, F. J. Aoiz, F. Lique, N. Marcelino, J. R. Goicoechea, M. González García, C. A. Gottlieb, M. C. McCarthy, and P. Thaddeus, Astron. Astrophys. 517, L2 (2010).
- ²¹ R. T. Desai, A. J. Coates, A. Wellbrock, V. Vuitton, F. J. Crary, D. González-Caniulef, O. Shebanits, G. H. Jones, G. R. Lewis, J. H. Waite, M. Cordiner, S. A. Taylor, D. O. Kataria, J.-E. Wahlund, N. J. T. Edberg, and E. C. Sittler, Astrophys. J. 844, L18 (2017).
- ²²V. Mukundan and A. Bhardwaj, Astrophys. J. **856**, 168 (2018).
- ²³S. S. Kumar, D. Hauser, R. Jindra, T. Best, Š. Roučka, W. D. Geppert, T. J. Millar, and R. Wester, Astrophys. J. 776, 25 (2013).
- ²⁴C. Meyer, A. Becker, K. Blaum, C. Breitenfeldt, S. George, J. Göck, M. Grieser, F. Grussie, E. Guerin, R. von Hahn, P. Herwig, C. Krantz, H. Kreckel, J. Lion, S. Lohmann, P. Mishra, O. Novotný, A. O'Connor, R. Repnow, S. Saurabh, D. Schwalm, L. Schweikhard, K. Spruck, S. S. Kumar, S. Vogel, and A. Wolf, Phys. Rev. Lett. 119, 023202 (2017).
- ²⁵ H. T. Schmidt, G. Eklund, K. C. Chartkunchand, E. K. Anderson, M. Kamińska, N. de Ruette, R. D. Thomas, M. K. Kristiansson, M. Gatchell, P. Reinhed, S. Rosén, A. Simonsson, A. Källberg, P. Löfgren, S. Mannervik, H. Zettergren, and H. Cederquist, Phys. Rev. Lett. 119, 073001 (2017).
- ²⁶E. K. Campbell, M. Holz, D. Gerlich, and J. P. Maier, Nature **523**, 322 (2015).
- ²⁷U. Fano and R. P. Rau, Atomic Collisions and Spectra (Elsevier, 1986).
- ²⁸D. A. Varshalovich, A. N. Moskalev, and V. K. Khersonskii, *Quantum Theory of Angular Momentum* (World Scientific, 1988).
- ²⁹ S. P. Davis, M. C. Abrams, M. L. P. Rao, and J. W. Brault, J. Opt. Soc. Am. B 8, 198 (1991).
- ³⁰C. A. Gottlieb, S. Brünken, M. C. McCarthy, and P. Thaddeus, J. Chem. Phys. 126, 191101 (2007).
- ³¹ R. Wester, J. Phys. B: At., Mol. Opt. Phys. **42**, 154001 (2009).
- ⁵²E. S. Endres, G. Egger, S. Lee, O. Lakhmanskaya, M. Simpson, and R. Wester, J. Mol. Spectrosc. **332**, 134 (2017).
- ³³R. Wester, Phys. Chem. Chem. Phys. **16**, 396 (2014).
- 34 J. Meyer and R. Wester, Annu. Rev. Phys. Chem. 68, 333 (2017).
- 35 E. Carrascosa, J. Meyer, and R. Wester, Chem. Soc. Rev. 46, 7498 (2017).
- ³⁶O. Lakhmanskaya, M. Simpson, S. Murauer, V. Kokoouline, and R. Wester, J. Chem. Phys. **149**, 104302 (2018).